Decoherence in large quantum registers under variable interaction with the environment

Marko Lovrić, Hans Georg Krojanski, and Dieter Suter
Universität Dortmund, Fachbereich Physik, 44221 Dortmund, Germany
(Received 7 December 2006; published 3 April 2007)

Effective quantum-information processing requires coherent control of large numbers of qubits on a time scale that is short compared to the decoherence time of the system. It is therefore important to extrapolate and measure decoherence times for large quantum registers and to determine the effect of different couplings between system and environment on the decoherence rate. For this purpose, we have experimentally realized a system that allows one to generate model quantum registers with more than 100 qubits and measure the decay of the information in these states while adjusting the strength of the interaction between the quantum register and the environment. Our results indicate a power-law dependence of the decoherence rate on the number of qubits in the system, with an exponent of the order of 0.5. This behavior remains qualitatively unchanged when the coupling strength to the environment is reduced by about an order of magnitude.

DOI: 10.1103/PhysRevA.75.042305 PACS number(s): 03.67.Lx, 03.65.Yz, 03.67.Pp

I. INTRODUCTION

Some computational problems are not efficiently solvable on classical computers, i.e., the computational time (or resources) grow exponentially with the size of the system [1]. Quantum computers use a different computational model and are therefore not subject to the same limitations. For some problems that are computationally hard on classical computers, it has been shown that quantum algorithms provide efficient solutions [2–4]. For most of these problems, a quantum computer that is able to implement these algorithms will have to consist of several hundreds to several thousands of qubits.

One of the main difficulties for realizing large-scale quantum-information processing is that the quantum information is much more fragile than classical information: The interaction with the environment entangles the quantum information with other degrees of freedom and therefore leads to a decay of the quantum information. This process is commonly referred to as decoherence. While decoherence has been characterized for small systems, it was unclear how it will affect quantum registers with a large number of qubits.

A number of schemes have been proposed for the design of scalable quantum-information processors [5–13], and some of these systems have been implemented with a small number of qubits [14–17]. However, to date no such implementation provides a large enough number of qubits that an extrapolation of decoherence rates would be possible. But decoherence rates can be measured in quantum mechanical systems that do not fulfill all the requirements for quantum-information processing [18]. Using nuclear spins in solids, it is possible to generate model quantum registers whose decoherence can be measured as a function of the register size up to several thousand qubits [19,20]. In this work, it was found that the decoherence rate increases roughly with the square root of the number of qubits.

Since imperfect gate operations and decoherence cannot be completely avoided, quantum error correction techniques have been developed [21]. To achieve reliable quantum-information processing with the help of these techniques, the failure probability of the quantum gates has to be smaller than a certain threshold [4]. If the decoherence in a system is too fast, a direct application of error correction schemes will not suffice. In such cases, the decoherence process due to the interaction with the environment can be reduced by introducing an additional time dependence on the quantum system [22,23]. In small systems such techniques are well known [24–31]. Recently we have shown that these techniques can also be used to decouple large quantum registers from their environment [20,32].

In these earlier experiments, the environment causing the decoherence was represented by the same spins that also formed the model quantum registers. It was therefore difficult to distinguish between system and environment.

To be able to manipulate the environment and its interaction with the quantum register without also affecting the qubits, we have implemented a different system. For this purpose, we use a system consisting of two different spin species, which we can address independently by resonant radio frequency fields. As indicated in Fig. 1 one nuclear spin species (the S spins) is used to implement the model quantum registers. The other species (the I spins) is responsible for the main perturbation that causes decoherence of the S spins. In the following, we will refer to these spins as the environment. This interaction can be controlled without manipulating the quantum register directly. Further we can vary the environment-qubit interaction strength between the natu-

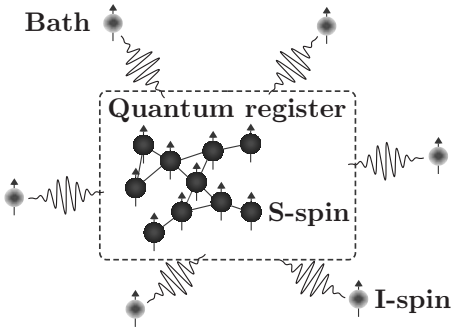

FIG. 1. Graphic illustration of a quantum register consisting of correlated spins (S), interacting with a different spin species (I) that represents the environment.

ral and a minimum level to examine the effect of the interaction on the scaling of the decoherence rates.

The main part of the paper is structured as follows. In Sec. II we discuss the relevant interactions in our system, the experimental scheme, and the creation of the model quantum registers. Section III deals with the decoherence measurements. It contains the method used for the decoherence measurements and the experimental results. In Sec. IV we summarize and discuss the results.

II. SYSTEM AND ENVIRONMENT

A. Qubits and interactions

We consider a system consisting of two different nuclear spin species. The S spins represent the qubits of the quantum register (see Fig. 1), while the I spins form the environment. The spins interact exclusively through the magnetic dipole-dipole coupling. The truncated Hamiltonian (with respect to the Zeeman interaction) of the full system and the environment is therefore [33]

$$\mathcal{H} = \mathcal{H}_{SS} + \mathcal{H}_{SI} + \mathcal{H}_{II}. \tag{1}$$

Among the qubits of the quantum register, which are identical spins, the relevant interaction Hamiltonian $\mathcal{H}_{SS}$ is the homonuclear dipole-dipole coupling

$$\mathcal{H}_{SS} = \sum_{i,j} \frac{d_{ij}^{SS}}{2}\left(2S_z^i S_z^j - \frac{S_+^i S_-^j + S_-^i S_+^j}{2}\right), \tag{2}$$

where d_{ij}^{SS} are the coupling constants (which depend on distance as r_{ij}^{-3}), S_z^i are the z components of the S^i spin operators and $S_\pm^i = S_x^i \pm i S_y^i$ are the corresponding raising and lowering operators. The homonuclear coupling Hamiltonian $\mathcal{H}_{II}$ for the I spins has the same form.

The system-environment interaction in this system is given by the heteronuclear dipolar coupling

$$\mathcal{H}_{IS} = \sum_{i,j} d_{ij}^{IS} I_z^i S_z^j. \tag{3}$$

In the system that we consider, the heteronuclear couplings represent the dominant interaction for the S spins.

The coupling with the environment can be made time dependent in a way that the average interaction vanishes. In the case of "bang-bang" decoupling, this is achieved by fast rotations applied to the qubits. In this system, we have the possibility of controlling not only the qubits, but also the environment: We apply a resonant radio frequency (rf) field to the I spins, which drives a rotation of the I spins and thereby continuously inverts the I_z term in Eq. (3) [26,34]. If the field is strong enough the rotation of the I spins becomes fast enough to average their effect on the S spin quantum register to zero. For the creation and description of the model quantum register that we describe in the following, we assume that this limiting case is reached and therefore omit the heteronuclear term in the Hamiltonian.

The eigenstates of $\mathcal{H}_{SS}$ can be classified by the total magnetic quantum number m_t of the total spin operator S_z,

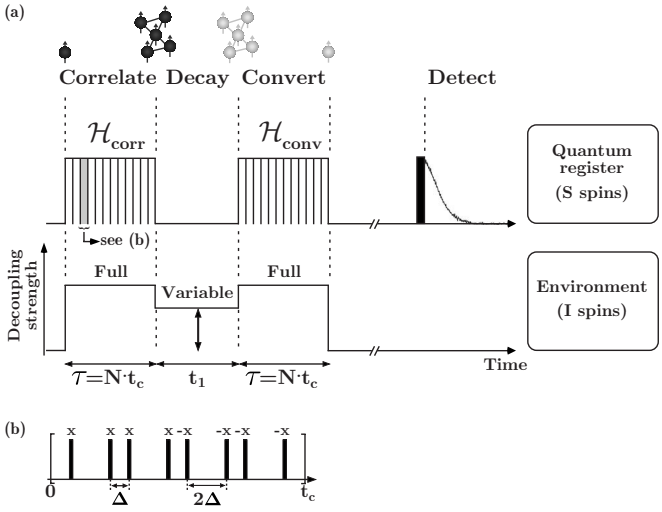

FIG. 2. (a) Experimental scheme: The upper part of the pulse sequence is applied to the quantum register spins whereas the lower one is used to decouple the S spins from the I spins. The effective Hamiltonians $\mathcal{H}_{corr}$ and $\mathcal{H}_{conv}$ are generated by a multiple pulse sequence that is repeated N times. The corresponding basic sequence of qubit rotations generating $\mathcal{H}_{corr}$ is shown in part (b); here $\times$ indicates a $\pi/2$ rotation around the x axis. The Hamiltonian $\mathcal{H}_{conv}$ converts the quantum information remaining after the interval t_1 into detectable magnetization. During the decay period t_1, we control the strength of the interaction between qubits and environment by varying the strength of the decoupling field between zero and full decoupling.

$$m_t = \sum_i m^i, \quad S_z = \sum_i S_z^i, \tag{4}$$

where m^i is the eigenvalue of S_z^i. In strongly dipolar coupled spin systems the eigenfunctions $|r\rangle$ of $\mathcal{H}_{SS}$ are eigenstates of S_z:

$$S_z|r\rangle = m_t^r|r\rangle. \tag{5}$$

The elements of the density operator ρ_S describing the system can therefore be labeled by the difference

$$M := m_t^r - m_t^s \tag{6}$$

of the total magnetic quantum number between the connected states $|r\rangle$ and $|s\rangle$, which is the coherence order M.

B. Quantum register

The S spin system is initially in thermal equilibrium and can be described by the high-temperature density operator

$$\rho_{S,\mathrm{eq}} = \frac{1}{2^N}\left(\mathbf{1} + \frac{\hbar \gamma_S B_0}{k_B T}\sum_{i=1}^{N} S_z^i\right) = \rho(0), \tag{7}$$

where N is the total number of S spins, γ_S their gyromagnetic ratio, B_0 the static magnetic field, and T the temperature. Each of the density operator terms depends only on a single spin; the different qubits are therefore uncorrelated.

To create correlations between the qubits, we use a multiple pulse sequence [see Fig. 2(b)], which converts the

homonuclear dipolar couplings $\mathcal{H}_{SS}$ to a suitable average Hamiltonian [35–37]

$$\mathcal{H}_{\text{corr}} = -\frac{1}{4}\sum_{i,j} d_{ij}^{SS}[S_+^i S_+^j + S_-^i S_-^j]. \tag{8}$$

To make sure that $\mathcal{H}_{\text{corr}}$ is the only relevant interaction, we have to eliminate the (heteronuclear) interaction $\mathcal{H}_{IS}$ with the environment. In the limit of short cycle times t_c, the pulse sequence of Fig. 2 satisfies this requirement [38,39]. But, in practice, we find it advantageous to use longer cycle times and therefore have to irradiate the I spins with a continuous rf field [26,34], which is sufficiently strong to ensure the limit of full decoupling.

As was shown in Ref. [35], the evolution under the influence of $\mathcal{H}_{\text{corr}}$ converts the initially independent spins to clusters of coupled spins, which serve as model quantum registers. The high order terms of the density operator series expansion,

$$\rho(\tau) = e^{-i\mathcal{H}_{\text{corr}}\tau}\rho(0)e^{i\mathcal{H}_{\text{corr}}\tau} \approx \rho(0) + i\tau[\rho(0),\mathcal{H}_{\text{corr}}] + \frac{i^2\tau^2}{2!}[[\rho(0),\mathcal{H}_{\text{corr}}],\mathcal{H}_{\text{corr}}] + \cdots, \tag{9}$$

of Eq. (9) contain terms that consist of products of many coupled spins. With increasing pump duration τ the contribution from terms with many spins increases. By choosing the number N of repetitions of the correlating multiple pulse sequence, one can vary the total duration $\tau = Nt_c$ and therefore the size of the resulting model quantum registers.

To detect the state of the quantum register after the decay period t_1 (see Fig. 2), one has to reconvert the excited multispin coherences into observable single spin coherences. This is achieved by letting the qubit system evolve under the effective Hamiltonian $\mathcal{H}_{\text{conv}} = -\mathcal{H}_{\text{corr}}$ for the same time τ [35,40]. Due to the simple behavior of $\mathcal{H}_{\text{corr}}$ under rotations around the z axis

$$e^{-i(\pi/2)S_z}\mathcal{H}_{\text{corr}}e^{i(\pi/2)S_z} = -\mathcal{H}_{\text{corr}} = \mathcal{H}_{\text{conv}}, \tag{10}$$

the pulse sequence that generates $\mathcal{H}_{\text{conv}}$ is the same as for $\mathcal{H}_{\text{corr}}$ except that the phases of all pulses are shifted by $\pi/2$. At the end of the reconversion the information about the state of the quantum register is stored as longitudinal magnetization. The readout is then accomplished by applying a $\pi/2$-rotation pulse and measuring the amplitude of the resulting free induction decay (FID).

C. Measuring the cluster size

To measure the size of the quantum registers, we use a method developed by Baum *et al.* [35]. To apply this technique, one needs to measure the amplitudes of all excited coherence orders M separately that contribute to the measured signal:

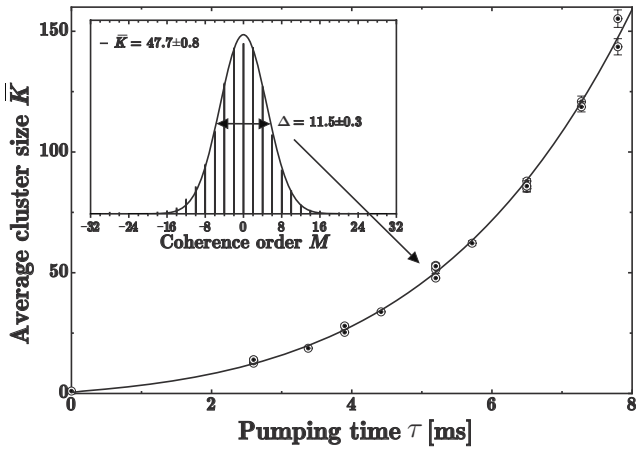

FIG. 3. Average spin cluster size $\bar{K}$ measured for different pumping times τ. The points represent measured spin cluster sizes with N ranging from 0 to 30 cycles of the basic pulse sequence (see Fig. 2) with $t_c = 259.872$ μs, measured without a decay period ($t_1 = 0$). The solid line serves as a guide to the eye. The inset shows a typical multiple quantum spectrum (for $N = 20$) with a Gaussian fit to obtain the cluster size. The graph comprises the results of several series of measurements.

$$\rho = \sum_M \rho_M. \tag{11}$$

In the following, we first determine the size of the clusters that are generated by the pumping process by performing this analysis for vanishing decay time, $t_1 = 0$.

Adding a phase ϕ to all pulses of the pumping sequence generating $\mathcal{H}_{\text{corr}}$ results in a rotation of the density operator by ϕ around the z axis. The density operator ρ_M then gains the phase factor $e^{iM\phi}$:

$$\rho(\tau,\phi) = e^{-i\phi S_z}\rho(\tau)e^{i\phi S_z} = \sum_M e^{iM\phi}\rho_M(\tau). \tag{12}$$

After reconversion with the help of $\mathcal{H}_{\text{conv}}$, as described in Sec. II B,

$$\rho(\tau+\tau,\phi) = e^{-i\mathcal{H}_{\text{conv}}\tau}\rho(\tau,\phi)e^{i\mathcal{H}_{\text{conv}}\tau}, \tag{13}$$

the longitudinal magnetization and therefore the signal becomes

$$S(\tau+\tau,\phi) = \text{Tr}[\rho(\tau)\rho(\tau,\phi)] = \sum_M S_M e^{iM\phi}. \tag{14}$$

The dependence on the rf pulse phase ϕ allows us to separate the signal into components arising from the coherence order M. For this purpose, we record a series of experiments with different values of ϕ. The resulting data set is Fourier-transformed with respect to ϕ [41,42]. The inset in Fig. 3 shows a typical resulting multiple quantum spectrum. The multiple quantum spectrum shows that, due to the bilinear raising and lowering operators, $\mathcal{H}_{\text{corr}}$ only excites even order coherences [35,37].

The statistical model of Ref. [35] assumes that, within the cluster that is generated, all allowed coherence orders are excited with the same probability during the pumping time τ. Under these assumptions the signal amplitudes in the mul-

tiple quantum spectrum are a direct measure for the number of the density operator elements with the coherence order M. The number n of possible M-quantum elements in a density operator that describes a system of K coupled spins-$\frac{1}{2}$ is given by the binomial distribution [43]

$$n(K,M) = \frac{(2K)!}{(K+M)!(K-M)!}, \tag{15}$$

which approximates to the Gaussian

$$n(K,M) \approx 2^{2K}(K\pi)^{-1/2} \exp\left(-\frac{M^2}{K}\right) \tag{16}$$

for sufficiently large K. The full width at half height (FWHH) of this distribution is $\Delta = 2\sqrt{\ln 2K}$. By fitting a Gaussian to the measured multiple quantum spectra we get the average number of coupled qubits $\bar{K}$ that form the model quantum register.

Figure 3 shows the dependence of the average cluster size $\bar{K}$ on the pumping time τ for a powdered sample of solid potassium hexafluorophosphate (KPF_6). Here the ^{31}P nuclei represent the qubit system (S spins) and the environment consists of the ^{19}F nuclei (I spins). The rise of the ^{31}P cluster size $\bar{K}$ in KPF_6 indicates a long-range dipolar coupled spin network typical for spin systems in solids [35]. The maximum cluster size of approximately 155 coupled spins reached with 8 ms of pumping time agrees with the expected values [38] for the given homonuclear dipolar coupling strengths between the ^{31}P nuclei in KPF_6 (see Sec. III B for experimental values).

The measurements were performed on a homebuilt solid-state NMR spectrometer with a proton resonance frequency of 300 MHz. Therefore, the resonance frequencies were 121.4 MHz for ^{31}P and 282.3 MHz for the ^{19}F nuclei. All measurements were performed at ambient temperature. The tuning of the homebuilt NMR double resonance probe was optimized with suitable tune-up pulse sequences [44–46] for best response to the multiple pulse sequences applied to ^{31}P. For the tune-up we used a dichlorobis(triethylphosphine) palladium(II) ($[(C_2H_5)_3P]_2PdCl_2$) sample of a size similar to the KPF_6 sample.

III. DECOHERENCE MEASUREMENTS

After the creation of the model quantum registers during the correlation period, it is possible to observe the loss of coherence by varying the decay time t_1 and measuring the signal amplitude left after the reconversion (see Fig. 2). The resulting signal

$$S(\tau + t_1 + \tau) = \mathrm{Tr}[\rho(\tau)\rho(\tau + t_1)] = f(\tau, t_1) \tag{17}$$

describes the decay of the information in the quantum register. For each measurement, the pumping time τ, which determines the quantum register size $\bar{K}$, was kept fixed.

Figure 4 shows the average signal decay for some typical quantum register sizes $\bar{K}$ in KPF_6, under the influence of the unmodified Hamiltonian $\mathcal{H}$, in comparison with the FID of the uncorrelated system. The data shows that large quantum registers lose stored information more rapidly than smaller ones, in agreement with the general expectation and our previous results obtained in a different system [19,20,32].

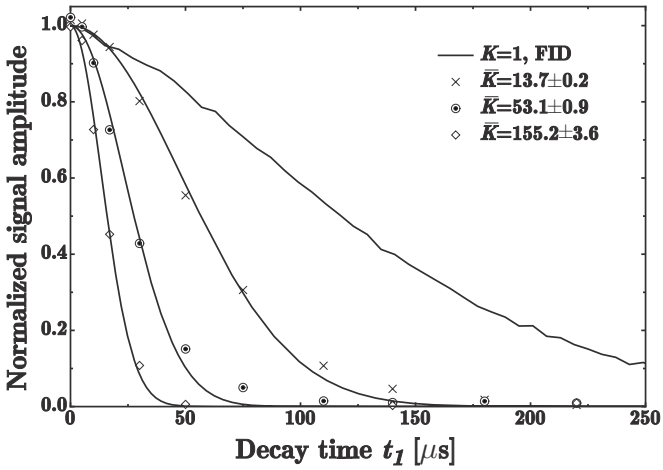

FIG. 4. The data sets show some decays for different quantum register sizes $\bar{K}$ starting from the FID and therefore uncorrelated qubits up to registers consisting of 155 qubits. Except for the FID the solid lines represent fits of the data to a Gaussian. All data sets have been normalized to their amplitudes at $t_1=0$. The coupling to the environment during t_1 was not averaged.

The solid lines represent Gaussian fits, which agree well with the observed shape of the decays and therefore will be used to quantify the decay rates. A theoretical approach to describe the shape of the decay more precisely for long decay times t_1, utilizing the effect of a partially correlated environment, can be found in [47].

A. Scaling of decoherence

To quantify the loss of coherence in different quantum register sizes we define a decoherence rate R as the inverse of the time $t_{1_{1/e}}$ for which the signal of Eq. (17) falls to $1/e$ of the initial value: $f(\tau, t_{1_{1/e}}) = f(\tau, t_1 = 0)/e$. As mentioned above, we approximate $f(\tau, t_1)$ by a Gaussian.

Figure 5 shows how the decoherence rates change with the size of the quantum register in KPF_6. The scaling approximates to a power function with exponent 0.56 and therefore qualitatively shows the same behavior as the results from Refs. [19,20,32] for a different physical system.

B. Dependence on coupling strength with environment

We now examine the effect of the strength of the coupling to the bath on the scaling of the decoherence rates. For this purpose, we apply decoupler fields of variable strength to the environmental spins I, which are here represented by ^{19}F nuclei. To achieve a full decoupling of the system from the environment, a decoupler field strength that exceeds the strength of the heteronuclear (^{31}P-^{19}F) couplings as well as that of the homonuclear (^{19}F-^{19}F) couplings is necessary. In our system we observe line broadenings (without decoupling) of approximate 3.3 kHz (FWHH) for the ^{31}P spectra

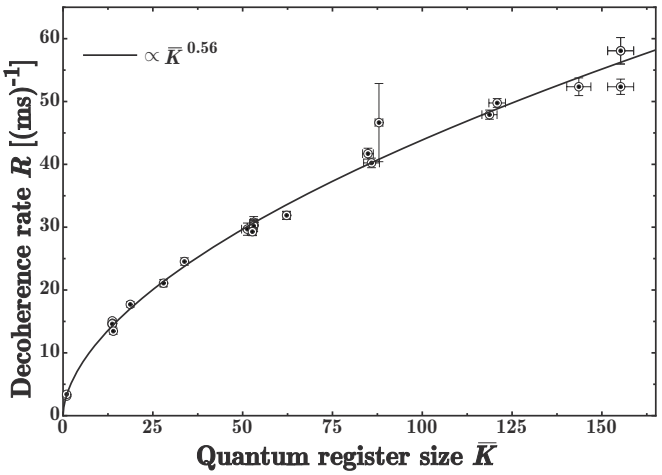

FIG. 5. Scaling of the decoherence rate for increasing quantum register size. In addition to the measured data points a power function fit to the data is shown as a solid line. The data shown summarizes more than one series of measurements.

and 11.9 kHz (FWHH) for the ^{19}F spectra due to the hetero- and homonuclear couplings mentioned in Sec. II. To exceed these values, we use maximum decoupler fields of up to $B_1^{\max}=93$ kHz $(2\pi/\gamma_I)$ (the constant factor will be omitted in the following).

Before discussing the effect of the decoupling on the highly correlated spin system, we show, as a reference, the effect of decoupling on the uncorrelated ^{31}P spins (see Fig. 6). Because the linewidth of the ^{31}P spectrum is about 3.3 kHz without decoupling, comparable fields applied to the ^{19}F nuclei can at least partially average the heteronuclear couplings [34]. Figure 6 shows that decoupling fields greater than approximately 7 kHz (in frequency units) are sufficient to average the ^{19}F-^{31}P couplings to zero. Experimental evidence and literature data [48,49] indicate that the dominant contribution to the remaining linewidth of 0.9 kHz (FWHH) of the ^{31}P spectrum is the dipole-dipole interaction between ^{31}P nuclear spins, which is not affected by the heteronuclear

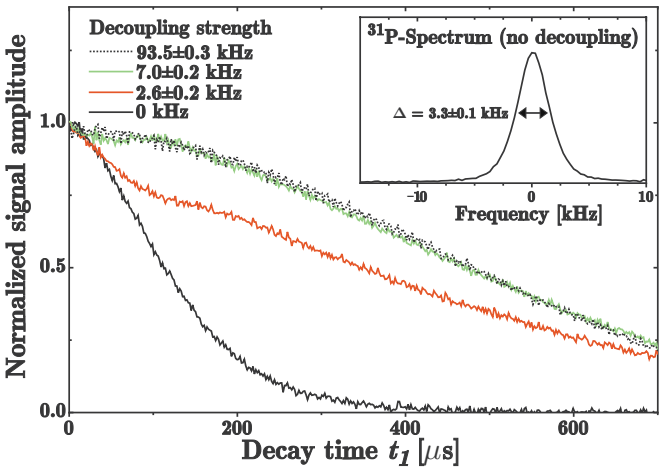

FIG. 6. (Color online) ^{31}P FIDs for different decoupling field strengths applied to ^{19}F. The inset shows the corresponding ^{31}P spectrum for the case of no decoupling.

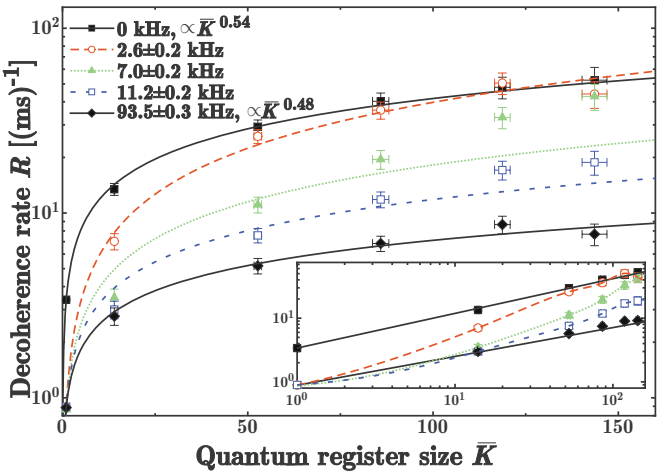

FIG. 7. (Color online) Scaling behavior of the decoherence rates R as a function of $\bar{K}$. The data shown compares the decoherence scaling for different decoupling strengths. The ^{19}F decoupling field strength is given as frequency. The lines drawn in the main plot correspond to power-function fits to the data. The inset shows a double-logarithmic plot of the same data and curves, except for the colored dashed lines which represent spline curves.

decoupling. In the regime of intermediate decoupling strength, the individual decay curves are no longer Gaussians. In this regime, the effective Hamiltonian that describes the interaction between system and bath in the presence of the decoupling field is time dependent, thus creating a more complicated decay function [34].

To examine the effect of decoupling on the decoherence of the quantum registers we now apply the decoupling field on the ^{19}F spins during the decay period t_1 of the experiment discussed above (see Fig. 2). The decoupling field strength during the correlation and reconversion was set to the maximal value of about 93 kHz. During t_1, we varied the decoupling field strength between 0 kHz and 93 kHz, which corresponds to a variation of the environment-qubit interaction between the maximum and essentially vanishing strength. Like in the case of individual spins, we found that the individual decay curves can be well approximated with Gaussians, but in the regime of intermediate decoupling, the time dependence becomes more complicated, with a small oscillatory component (whose frequency corresponds to the field strength of the decoupling field). Therefore, we determined the decay times from the integral of the decay curves.

Figure 7 shows the scaling behavior of the decoherence rates R as a function of the register size $\bar{K}$ for different degrees of decoupling from the environment. For the cases of free evolution and a fully decoupled environment (the black lines and points), the data can be fitted quite well with a power law, $R \propto \bar{K}^p$. The fitted exponents ($p=0.54\pm0.01$ for no decoupling and $p=0.48\pm0.01$ for the strongest decoupling field) indicate that the full decoupling is even more effective for larger spin clusters. The same behavior was also observed in the homonuclear system of Refs. [20,32], where only the cases of full and essentially no coupling between system and environment could be investigated.

In the intermediate range of decoupling strengths that we can observe in our system, the scaling of the rates R with $\bar{K}$

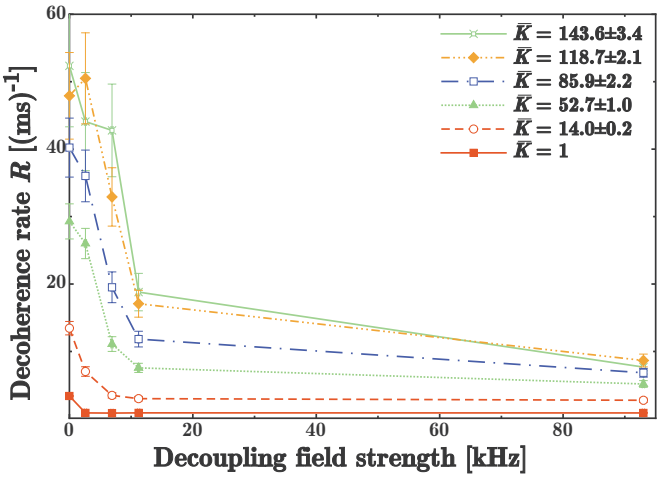

FIG. 8. (Color online) Decoherence rates R for different register sizes $\bar{K}$ as a function of the decoupling field strength. Data points belonging to the same register size have been connected with straight lines.

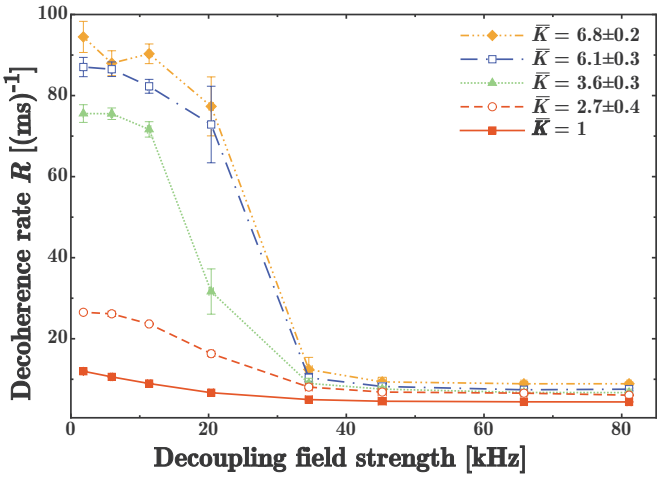

FIG. 9. (Color online) Shows the same plots as Fig. 8 but with ^{13}C data obtained from labeled glycine ($H_2N^*CH_2COOH$).

shows a different behavior. The data does not fit anymore to the simple empirical power law, as can be seen in Fig. 7. For example, the decoherence rates for large registers show higher values than would be expected from a simple power-law dependence. To emphasize this, the inset of Fig. 7 shows a double-logarithmic plot, where the data points belonging to an intermediate decoupling field strength have been connected with a spline curve. The black lines in the inset show the straight lines resulting from the power-function fits of the extreme cases of zero and maximum decoupling field strength. In contrast to the extreme cases, the decay rates in the intermediate decoupling range cannot be connected by straight lines. This is not too surprising, since in this regime not only the strength of the interaction between system and environment is changing, but also the correlation times of the interaction. This different behavior is also evident in the individual decay curves, as discussed earlier in this section.

Figure 8 shows the same data as a function of the decoupling field strength for fixed quantum register sizes. For sufficiently high decoupler fields, the decay rate R for each register size $\bar{K}$ reaches a limiting value. Further it indicates that the decoherence rates of small quantum registers reach this plateau faster than those of the large registers. Furthermore, the increase of the decoherence rates for the large quantum registers is steeper and starts at higher decoupling field strengths. Qualitatively this is the same behavior as for the single spin case, where a certain threshold for the decoupling field has to be reached from which the system seems to be fully decoupled. The more rapid increase of the decoherence rates and the observation that this raising starts at higher decoupling fields indicates a higher threshold for large quantum registers.

Figure 7 also contains this information. The difference of the decoherence rates for full and vanishing decoupling strength remain mostly the same comparing different quantum register sizes. In contrast, the difference of the R values for zero and an intermediate decoupling strength (e.g., the lower black points and the green points) change from one register size to the other. The rates increase more rapidly for a lower degree of decoupling until they ultimately reach the limiting values for no decoupling. This maximum level of R is reached faster for large quantum registers, when the decoupling decreases (compare the upper black curve and the red points). Therefore, the scaling behavior observed in the intermediate regime of decoupling indicates that the threshold is significantly higher for larger spin clusters. Once this threshold is exceeded (for the largest observed or created register), the overall scaling seems to approximate the previously observed power law scaling.

The described behavior could also be observed in a different chemical system. We have performed similar experiments in ^{13}C-labeled glycine ($H_2N^*CH_2COOH$). Here the quantum register was created within the ^{13}C spin system. In this system, the couplings between the qubits are weaker than in the previously discussed system, whereas the coupling to the controllable environment, the ^{1}H spins, is stronger. Because of the lower symmetry in this system, the chemical shielding anisotropy does not vanish. We therefore had to use a modified pulse sequence [50] during the correlation and reconversion period to eliminate this unwanted interaction.

The weak homonuclear dipolar couplings and the less efficient correlating pulse sequence inhibit the creation of large model quantum registers in this system. The maximum register size obtained in our experiments was about $\bar{K}=7$. Figure 9 shows the decoherence rates R of the ^{13}C-quantum registers of glycine as a function of the decoupling field strength that was applied to the ^{1}H environment. Even though we did not reach similar quantum register sizes within glycine we see qualitatively the same behavior as in KPF_6.

IV. DISCUSSION AND CONCLUSION

For the measurements of decoherence rates in quantum registers of different sizes, we have used highly correlated spin states in a system of two different spin species in two different physical systems. One of these spins served as a

model for the quantum register, while the second species, which we can control independently, represents the environment causing the decoherence of the quantum information. This allowed us to study the decoherence in systems of up to 150 qubits as a function of the system size as well as a function of the strength of the coupling to the environment.

Our system does not allow us to measure individual decoherence rates of specific elements or states of the quantum register. Instead, we measure an average decay corresponding to the autocorrelation function of the initial quantum state. Such an average decoherence rate is the relevant quantity for the discussion of the loss of information in large-scale quantum computers: During the execution of a quantum algorithm, the information is repeatedly redistributed over the whole Hilbert space of the quantum register and therefore decays with an averaged rate determined by all the individual rates as well as by the quantum algorithm.

Our experimental results show that the decoherence rate increases roughly with the square root of the number of qubits, in good agreement with earlier measurements [19,20,32]. The modulation scheme that we imposed on the environment proved effective for reducing the decay rate for all system sizes. This result, which verifies earlier measurements in different systems, indicates that the prospects for large scale quantum computers may be better than expected.

If the perturbations that influence the different qubits are uncorrelated one would generally expect a linear scaling of the decoherence [51,52]. Thus the less-than-linear scaling of the decoherence rates indicates that the perturbations here are correlated. This is certainly a consequence of the finite range of the interactions that cause the decoherence. Reference [47] provides a theoretical approach which utilizes correlated perturbations to describe the shape of the decay curves like that shown in Fig. 4 and further provides the power-law scaling of the decoherence rates.

The data for KPF_6 and glycine (see Figs. 8 and 9) indicate that effective decoupling becomes possible only when the strength of the decoupling field exceeds a certain threshold, which increases with the quantum register size. This may indicate that the degree of decoupling that can be realized in a physical system will limit the practical size of the quantum register.

The heteronuclear system used in this study allows also the investigation of another aspect: While the environmental degrees of freedom were strongly coupled in these experiments (by $\mathcal{H}_{II}$), it would be possible to eliminate this coupling by a modified decoupling scheme using off-resonant irradiation [53,54]. In this way, it would become possible to study the effect of the correlation time in the environment on the decoherence in the quantum register. This effect could be studied independently of the dependence on the strength of the coupling.

ACKNOWLEDGMENTS

The financial support of this work by the Deutsche Forschungsgemeinschaft through the Graduiertenkolleg 726 is gratefully acknowledged.

[1] R. P. Feynman, Int. J. Theor. Phys. **21**, 467 (1982).
[2] P. W. Shor, in *Proceedings of the 35th Annual Symposium on the Foundations of Computer Science*, edited by S. Goldwasser (IEEE Computer Society Press, Los Alamitos, CA, 1994), p. 124.
[3] D. P. DiVincenzo, Science **270**, 255 (1995).
[4] M. A. Nielsen and I. L. Chuang, *Quantum Computation and Quantum Information* (Cambridge University Press, Cambridge, UK, 2000).
[5] J. E. Mooij, T. P. Orlando, L. Levitov, L. Tian, C. H. van der Waal, and S. Lloyd, Science **285**, 1036 (1999).
[6] D. Loss and D. P. DiVincenzo, Phys. Rev. A **57**, 120 (1998).
[7] J. I. Cirac and P. Zoller, Phys. Rev. Lett. **74**, 4091 (1995).
[8] B. Kane, Nature (London) **393**, 133 (1998).
[9] D. G. Cory *et al.*, Fortschr. Phys. **48**, 875 (2000).
[10] R. Vrijen, E. Yablonovitch, K. Wang, H. W. Jiang, A. Balandin, V. Roychowdhury, T. Mor, and D. DiVincenzo, Phys. Rev. A **62**, 012306 (2000).
[11] D. Suter and K. Lim, Phys. Rev. A **65**, 052309 (2002).
[12] T. D. Ladd, J. R. Goldman, F. Yamaguchi, Y. Yamamoto, E. Abe, and K. M. Itoh, Phys. Rev. Lett. **89**, 017901 (2002).
[13] M. Mehring and J. Mende, Phys. Rev. A **73**, 052303 (2006).
[14] M. Riebe, K. Kim, P. Schindler, T. Monz, P. O. Schmidt, T. K. Korber, W. Hansel, H. Haffner, C. F. Roos, and R. Blatt, Phys. Rev. Lett. **97**, 220407 (2006).
[15] M. Grajcar *et al.*, Phys. Rev. Lett. **96**, 047006 (2006).
[16] Y. Wu, X. Li, L. M. Duan, D. G. Steel, and D. Gammon, Phys. Rev. Lett. **96**, 087402 (2006).
[17] F. H. L. Koppens, C. Buizert, K. J. Tielrooij, I. T. Vink, K. C. Nowack, T. Meunier, L. P. Kouwenhoven, and L. M. K. Vandersypen, Nature (London) **442**, 766 (2006).
[18] D. P. DiVincenzo, Fortschr. Phys. **48**, 771 (2000).
[19] H. G. Krojanski and D. Suter, Phys. Rev. Lett. **93**, 090501 (2004).
[20] H. G. Krojanski and D. Suter, Phys. Rev. Lett. **97**, 150503 (2006).
[21] J. Preskill, Proc. R. Soc. London, Ser. A **454**, 385 (1998).
[22] L. Viola and S. Lloyd, Phys. Rev. A **58**, 2733 (1998).
[23] P. Facchi, S. Tasaki, S. Pascazio, H. Nakazato, A. Tokuse, and D. A. Lidar, Phys. Rev. A **71**, 022302 (2005).
[24] E. L. Hahn, Phys. Rev. **80**, 580 (1950).
[25] H. Y. Carr and E. M. Purcell, Phys. Rev. **94**, 630 (1954).
[26] L. R. Sarles and R. M. Cotts, Phys. Rev. **111**, 853 (1958).
[27] S. Meiboom and D. Gill, Rev. Sci. Instrum. **29**, 688 (1958).
[28] J. S. Waugh, L. M. Huber, and U. Haeberlen, Phys. Rev. Lett. **20**, 180 (1968).
[29] E. Fraval, M. J. Sellars, and J. J. Longdell, Phys. Rev. Lett. **95**, 030506 (2005).
[30] T. D. Ladd, D. Maryenko, Y. Yamamoto, E. Abe, and K. M. Itoh, Phys. Rev. B **71**, 014401 (2005).
[31] J. Baugh, O. Moussa, C. A. Ryan, R. Laflamme, C. Ramanathan, T. F. Havel, and D. G. Cory, Phys. Rev. A **73**,

022305 (2006).
[32] H. G. Krojanski and D. Suter, Phys. Rev. A **74**, 062319 (2006).
[33] A. Abragam, *Principles of Nuclear Magnetism* (Oxford Science Publications, Oxford, 1994).
[34] M. Mehring, *High Resolution NMR Spectroscopy in Solids* (Springer-Verlag, Berlin, 1976).
[35] J. Baum, M. Munowitz, A. N. Garroway, and A. Pines, J. Chem. Phys. **83**, 2015 (1985).
[36] W. S. Warren, S. Sinton, D. P. Weitekamp, and A. Pines, Phys. Rev. Lett. **43**, 1791 (1979).
[37] W. S. Warren, D. P. Weitekamp, and A. Pines, J. Chem. Phys. **73**, 2084 (1980).
[38] B. E. Scruggs and K. K. Gleason, J. Magn. Reson. (1969-1992) **99**, 149 (1991).
[39] B. C. Gerstein and C. R. Dybowski, *Transient Techniques in NMR of Solids* (Academic Press, Orlando, 1985).
[40] Y.-S. Yen and A. Pines, J. Chem. Phys. **78**, 3579 (1983).
[41] S. Emid, Physica B & C **128**, 79 (1985).
[42] D. N. Shykind, J. Baum, S.-B. Liu, A. Pines, and A. N. Garroway, J. Magn. Reson. (1969-1992) **76**, 149 (1988).
[43] A. Wokaun and R. R. Ernst, Mol. Phys. **36**, 317 (1978).
[44] M. Mehring and J. S. Waugh, Rev. Sci. Instrum. **43**, 649 (1972).
[45] U. Haubenreisser and B. Schnabel, J. Magn. Reson. (1969-1992) **35**, 175 (1979).
[46] D. P. Burum, M. Linder, and R. R. Ernst, J. Magn. Reson. (1969-1992) **43**, 463 (1981).
[47] A. Fedorov and L. Fedichkin, J. Phys.: Condens. Matter **18**, 3217 (2006).
[48] G. R. Miller and H. S. Gutowsky, J. Chem. Phys. **39**, 1983 (1963).
[49] R. Challoner, T. Schaller, and A. Sebald, J. Magn. Reson., Ser. A **101**, 106 (1993).
[50] O. N. Antzutkin and R. Tycko, J. Chem. Phys. **110**, 2749 (1999).
[51] W. G. Unruh, Phys. Rev. A **51**, 992 (1995).
[52] G. M. Palma, K.-A. Suominen, and A. K. Ekert, Proc. R. Soc. London, Ser. A **452**, 567 (1996).
[53] W. I. Goldburg and M. Lee, Phys. Rev. Lett. **11**, 255 (1963).
[54] M. Lee and W. I. Goldburg, Phys. Rev. **140**, A1261 (1965).